OUSSAMA AJALA [*], *DIETER BESTLE* [**], *JOCHEN RAUH* [*]

MODELLING AND CONTROL OF AN ELECTRO-HYDRAULIC ACTIVE SUSPENSION SYSTEM

Active suspension systems ease the conflict between comfort and handling. This requires the use of suitable actuators that in turn need to be efficiently controlled. This paper proposes a model-based control approach for a nonlinear suspension actuator. Firstly the concept is derived in the linear framework in order to simplify the synthesis and analysis phase. There a linear model of the actuator is proposed and discussed. Further, this design phase includes a comparison between model-free PID controllers and a newly proposed two-degree-of-freedom controller which allows one to shape reference and disturbance responses separately. Subsequently, the two-degree-of-freedom controller, which proves to be superior, is adapted to the nonlinear framework by considering a linear parameter varying representation of the nonlinear plant. Finally, the nonlinear controller is implemented in a test car confirming the concept applicability to real hardware.

1. Introduction

Ride and handling characteristics of passenger cars are mainly influenced by the suspension system. The design of suspension systems using passive components always involves a trade-off between the conflicting criteria characterizing road handling and passenger comfort. Active suspensions implemented with sensors, controllers, actuators and a data processing unit, however, make it possible to apply additional suspension forces on demand and in this way reduce the conflict between comfort, handling and safety. The control system of such suspensions usually involves two levels. On the upper level, the car body controller determines additive forces needed for the actual driving condition, where different control approaches have been

[*] *Group Res. & Adv. Eng. Vehicle Dynamics Daimler AG 050/G005, 71059 Sindelfingen, Germany; E-mail: oussama.ajala@daimler.com; E-mail: jochen.rauh@daimler.com*

[**] *Engineering Mechanics and Vehicle Dynamics, Brandenburg University of Technology, 03046 Cottbus, Germany; E-mail: bestle@tu-cottbus.de*

investigated ranging from the simple skyhook controller to more complicated optimal controller design methods [1], [2]. On the lower level, the actuator controller has to guarantee that the actuator achieves the desired reference force provided by the car body controller. Most of the research conducted on active suspension systems (e.g. [3]-[6]) considers the actuator as an ideal force source and neglects its internal dynamics that interacts in many ways with the rest of the vehicle dynamics. In fact, most of the actuators exhibit nonlinear behaviour [7], have a limited bandwidth [8], and are exposed to external disturbances which makes the controller design more complicated and sets additional requirements on the controller design process. Moreover, the realisation of active suspensions has been often the focus of just theoretical investigations with little connection to practical implementation.

Therefore, this paper focuses on the development of an actuator controller for an existing active suspension system and is organized as follows. In section 2, the nonlinear actuator model is presented and the derivation of a simplified linear model is explained. Two different control strategies comprising a pure feedback control and a two-degree-of-freedom (2-DOF) scheme, which combines feedback and feed-forward strategies, are introduced in section 3. The approach is based on a linear control design methodology in order to permit frequency-domain analysis. Here the linear framework is used as an intermediate model description in the process of synthesizing a controller for the nonlinear model. The final nonlinear controller and results from the experimental setup are then presented in section 4. The proposed control approach is implemented in a real test car to confirm its performance and the aptitude to be used in practice. The real car measurements are discussed in section 5.

2. System description and modeling

The actuator in Fig. 1a comprises a conventional shock absorber cylinder, two controllable valves to generate unidirectional damping resistance, and two accumulators that compensate the volume change in the cylinder chambers. In this configuration, the actuator operates exactly like a passive spring-damper element. In order to be able to exert active forces, i.e. independently of the amplitude and sign of deflection velocities $\dot{z}_e$, a power-pack comprising a hydraulic pump and an electric motor is added.

2.1. Nonlinear mathematical model

Accumulators store hydraulic energy and then provide this energy back to the system when required. Assuming a polytropic change of gas state, the
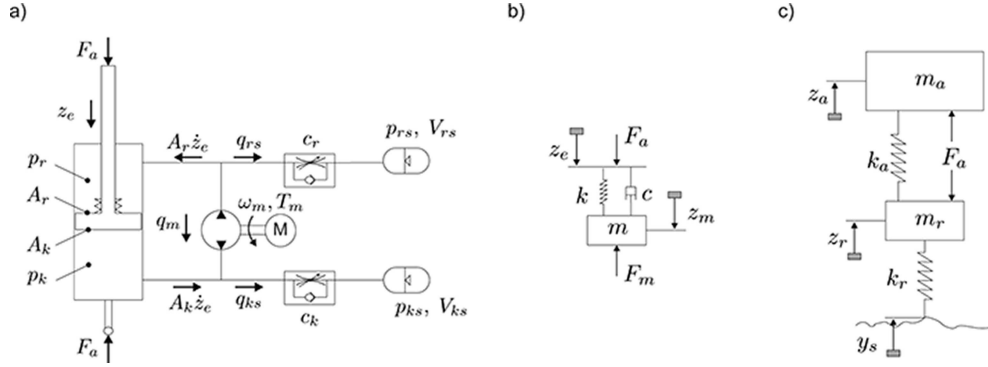
Fig. 1. Nonlinear actuator model (a) according to [9], linearised actuator model (b), and application to a quarter-car model (c)

following state equation for the pressure in the lower accumulator in Fig. 1a can be obtained:

$$p_{ks}V_{ks}^{\kappa} = p_0 V_{k0}^{\kappa} \quad \text{or} \quad p_{ks} = p_0 \left(\frac{V_{k0}}{V_{ks}}\right)^{\kappa} \tag{1}$$

where p_0 is the static charge pressure, V_{k0} is the initial gas volume, $V_{ks} = V_{k0} - \int q_{ks}dt$ is the actual gas volume due to fluid flow q_{ks}, and κ is the polytropic gas constant. Differentiating (1) with respect to time and substituting $\dot{V}_{ks} = -q_{ks}$ yields the state equation of the pressure rate of change

$$\dot{p}_{ks} = p_0\kappa \left(\frac{V_{k0}}{V_{ks}}\right)^{\kappa-1} \left(-\frac{V_{k0}}{V_{ks}^2}\dot{V}_{ks}\right) = \kappa p_0 \left(\frac{V_{k0}}{V_{ks}}\right)^{\kappa} \left(\frac{-\dot{V}_{ks}}{V_{ks}}\right) = \kappa \, q_{ks}\frac{p_{ks}}{V_{ks}}. \tag{2}$$

Analogously, the state equation for the upper gas accumulator in Fig. 1a is

$$\dot{p}_{rs} = \kappa q_{rs}\frac{p_{rs}}{V_{rs}}. \tag{3}$$

The equation of motion of the pump reads as

$$J_m\dot{\omega}_m = T_m - \frac{V_c}{2\pi}(p_k - p_r) \tag{4}$$

where ω_m is the angular velocity of the pump, J_m is the total mass moment of inertia of motor and pump, V_c is the pump capacity coefficient, p_k and p_r are the cylinder pressures, and T_m is the motor torque. If the internal leakage flow is neglected, the pump flow is

$$q_m = \frac{V_c}{2\pi}\,\omega_m. \tag{5}$$

The actuator force is calculated from both pressures acting on the piston:

$$F_a = p_k A_k - p_r A_r = (p_{ks} + \Delta p_{ks}) A_k - (p_{rs} + \Delta p_{rs}) A_r \qquad (6)$$

where A_k and A_r are the surfaces of the piston in the two respective cylinder chambers. The pressure drops Δp_{ks} and Δp_{rs} result from the damping valves as

$$\Delta p_{ks} = p_k - p_{ks} = q_{ks} c_k, \quad \Delta p_{rs} = p_r - p_{rs} = q_{rs} c_r \qquad (7)$$

where

$$c_k = c_k (q_{ks}), \quad c_r = c_r (q_{rs}) \qquad (8)$$

are the nonlinear characteristics of the valves depending on the flows through the valves. The characteristics correspond to those of valves used in conventional shock absorbers. With the suspension deflection z_e, the internal fluid flows in the actuator are balanced to

$$q_{ks} = q_m + \dot{z}_e A_k, \quad q_{rs} = -q_m - \dot{z}_e A_r. \qquad (9)$$

Substituting q_{ks} from (9) and q_m from (5) in (2) yields

$$\dot{p}_{ks} = \kappa \ (q_m + \dot{z}_e A_k) \frac{p_{ks}}{V_{ks}} = \kappa \ \left(\frac{V_c}{2\pi} \omega_m + \dot{z}_e A_k \right) \frac{p_{ks}}{V_{ks}}. \qquad (10)$$

Similarly, substitution q_{rs} from (9) and (5) in (3) results in

$$\dot{p}_{rs} = \kappa \ (-q_m - \dot{z}_e A_r) \frac{p_{rs}}{V_{rs}} = -\kappa \ \left(\frac{V_c}{2\pi} \omega_m + \dot{z}_e A_r \right) \frac{p_{rs}}{V_{rs}}. \qquad (11)$$

From equations (4) and (7) we obtain

$$\dot{\omega}_m = \frac{1}{J_m} \ \left(T_m - \frac{V_c}{2\pi} (p_{ks} - p_{rs}) - \frac{V_c}{2\pi} (q_{ks} \ c_k - q_{rs} \ c_r) \right), \qquad (12)$$

or after use of (9) and (5) we obtain

$$\dot{\omega}_m = \frac{1}{J_m} \ \left(T_m - \frac{V_c}{2\pi} (p_{ks} - p_{rs}) - \left(\frac{V_c}{2\pi} \right)^2 \ (c_k + c_r) \ \omega_m - \frac{V_c}{2\pi} (c_k A_k + c_r A_r) \ \dot{z}_e \right). \qquad (13)$$

The output force of the actuator results from (6) and (7) as

$$F_a = (A_k p_{ks} - A_r p_{rs}) + A_k \ c_k \ q_{ks} - A_r \ c_r \ q_{rs} \qquad (14)$$

or after substitution of (9) and (5) as

$$F_a = (A_k p_{ks} - A_r p_{rs}) + A_k \ c_k \ (q_m + \dot{z}_e A_k) + A_r \ c_r \ (q_m + \dot{z}_e A_r)$$
$$= (A_k p_{ks} - A_r p_{rs}) + (c_k A_k + c_r A_r) \frac{V_c}{2\pi} \omega_m + \left(c_k A_k^2 + c_r A_r^2 \right) \dot{z}_e. \qquad (15)$$

After introducing the state vector $\boldsymbol{x} = \begin{bmatrix} p_{ks} & p_{rs} & \omega_m \end{bmatrix}^T$, input vector $\boldsymbol{u} = \begin{bmatrix} \dot{z}_e & T_m \end{bmatrix}^T$, and output vector $\boldsymbol{y} = \begin{bmatrix} F_a \end{bmatrix}$, the state equations of the nonlinear actuator model read as

$$\dot{\boldsymbol{x}} = \boldsymbol{f}(\boldsymbol{x}, \boldsymbol{u}), \quad \boldsymbol{y} = \boldsymbol{g}(\boldsymbol{x}, \boldsymbol{u}) \tag{16a}$$

where

$$\boldsymbol{f} = \begin{bmatrix} \kappa \left(\dfrac{V_c}{2\pi} \omega_m + \dot{z}_e A_k \right) \dfrac{p_{ks}}{V_{ks}} \\[2mm] -\kappa \left(\dfrac{V_c}{2\pi} \omega_m + \dot{z}_e A_r \right) \dfrac{p_{rs}}{V_{rs}} \\[2mm] \dfrac{1}{J_m} \left(-\dfrac{V_c}{2\pi} (p_{ks} - p_{rs}) - \left(\dfrac{V_c}{2\pi} \right)^2 (c_k + c_r) \omega_m - \dfrac{V_c}{2\pi} (c_k A_k + c_r A_r) \dot{z}_e \right) + \dfrac{T_m}{J_m} \end{bmatrix},$$

$$\boldsymbol{g} = A_k p_{ks} - A_r p_{rs} + \frac{V_c}{2\pi} (c_k A_k + c_r A_r) \omega_m + \left(c_k A_k^2 + c_r A_r^2 \right) \dot{z}_e \tag{16b}$$

summarize equations (10), (11), (13) and (15).

2.2. Model linearization and order reduction

The equilibrium state $\boldsymbol{x}_0 = const.$ of system (16) results from $\dot{\boldsymbol{x}}_0 = \boldsymbol{f}(\boldsymbol{x}_0, \boldsymbol{u}_0) \overset{!}{=} \boldsymbol{0}$ with reference input $\boldsymbol{u}_0 = \begin{bmatrix} \dot{z}_{e0} & T_{m0} \end{bmatrix}^T = \begin{bmatrix} 0 & 0 \end{bmatrix}^T$ and $\omega_m = 0$. The static pressures $p_{ks} = p_{rs}$ may be set to p_0, i.e. $\boldsymbol{x}_0 = \begin{bmatrix} p_{ks0} & p_{rs0} & \omega_{m0} \end{bmatrix}^T = \begin{bmatrix} p_0 & p_0 & 0 \end{bmatrix}^T$. From (15) the static actuator force then results in $F_{a0} = (A_k - A_r) p_0$.

Considering equations (8) and (9) about the equilibrium point $q_{m0} = (V_c/2\pi) \omega_{m0} = 0$ and $\dot{z}_{e0} = 0$, the damping coefficients are set to $c_{k0} = c_k(0)$ and $c_{r0} = c_r(0)$. Using the Taylor series expansion of the nonlinear equations and truncating after the linear terms with respect to state and input deviations from stationary values, we obtain the linear model

$$\begin{aligned} \dot{\hat{\boldsymbol{x}}} &= \hat{\boldsymbol{A}} \hat{\boldsymbol{x}} + \hat{\boldsymbol{B}} \boldsymbol{u}, \\ \hat{\boldsymbol{y}} &= \hat{\boldsymbol{C}} \hat{\boldsymbol{x}} + \hat{\boldsymbol{D}} \boldsymbol{u} \end{aligned} \tag{17a}$$

where

$$\hat{x} = x - x_0 = \begin{bmatrix} p_{ks} - p_0 & p_{rs} - p_0 & \omega_m \end{bmatrix}^T, \quad \hat{y} = F_a - F_{a0},$$

$$\hat{A} = \begin{bmatrix} 0 & 0 & \kappa \dfrac{V_c}{2\pi} \dfrac{p_0}{V_{k0}} \\[2ex] 0 & 0 & -\kappa \dfrac{V_c}{2\pi} \dfrac{p_0}{V_{r0}} \\[2ex] -\dfrac{V_c}{2\pi J_m} & \dfrac{V_c}{2\pi J_m} & -\left(\dfrac{V_c}{2\pi}\right)^2 \dfrac{c_{k0} + c_{r0}}{J_m} \end{bmatrix}, \quad \hat{B} = \begin{bmatrix} \kappa A_k \dfrac{p_0}{V_{k0}} & 0 \\[2ex] -\kappa A_r \dfrac{p_0}{V_{r0}} & 0 \\[2ex] -\dfrac{V_c}{2\pi} \dfrac{(c_{k0} A_k + c_{r0} A_r)}{J_m} & \dfrac{1}{J_m} \end{bmatrix},$$

$$\hat{C} = \begin{bmatrix} A_k & -A_r & \dfrac{V_c}{2\pi}(c_{k0}A_k + c_{r0}A_r) \end{bmatrix}, \qquad \hat{D} = \begin{bmatrix} \left(c_{k0}A_k^2 + c_{r0}A_r^2\right) & 0 \end{bmatrix}.$$
(17b)

Analyzing system matrix $\hat{A}$ and input matrix $\hat{B}$, we notice that the equations for the pressures $(p_{ks} - p_0)$ and $(p_{rs} - p_0)$ are linearly dependent. Therefore, we introduce the simple state variable $\Delta p = p_{ks} - p_{rs}$. Further, we assume that the areas A_k and A_r are equal and substitute them by A_0. System (17) can be then reduced to a system of dimension two:

$$\dot{x}_r = A_r x_r + B_r u,$$
$$y_r = C_r x_r + D_r u$$
(18a)

where

$$x_r = \begin{bmatrix} \Delta p & \omega_m \end{bmatrix}^T, \qquad\qquad y_r = F_a - F_{a0},$$

$$A_r = \begin{bmatrix} 0 & \kappa \dfrac{V_c}{2\pi}\left(\dfrac{p_0}{V_{k0}} + \dfrac{p_0}{V_{r0}}\right) \\[2ex] -\dfrac{V_c}{2\pi J_m} & -\left(\dfrac{V_c}{2\pi}\right)^2 \dfrac{c_{k0} + c_{r0}}{J_m} \end{bmatrix}, \quad B_r = \begin{bmatrix} \kappa A_0 \left(\dfrac{p_0}{V_{k0}} + \dfrac{p_0}{V_{r0}}\right) & 0 \\[2ex] -\dfrac{V_c}{2\pi} \dfrac{A_0(c_{k0} + c_{r0})}{J_m} & \dfrac{1}{J_m} \end{bmatrix},$$

$$C_r = \begin{bmatrix} A_0 & \dfrac{V_c}{2\pi} A_0(c_{k0} + c_{r0}) \end{bmatrix}, \qquad D_r = \begin{bmatrix} A_0^2(c_{k0} + c_{r0}) & 0 \end{bmatrix}.$$
(18b)

2.3. Equivalent mechanical system and quarter-car model

Application of the Laplace transformation to the system equations (18) yields

$$\mathcal{L}\{\Delta \dot{p}(t)\} = s\Delta p(s) = \kappa \frac{V_c}{2\pi}\left(\frac{p_0}{V_{k0}} + \frac{p_0}{V_{r0}}\right)\omega_m + \kappa A_0 \left(\frac{p_0}{V_{k0}} + \frac{p_0}{V_{r0}}\right)s z_e, \quad (19)$$

$$\mathcal{L}\{\dot{\omega}_m(t)\} = s\omega_m(s) = -\frac{V_c}{2\pi J_m}\Delta p - \left(\frac{V_c}{2\pi}\right)^2 \frac{c_{k0}+c_{r0}}{J_m}\omega_m - \frac{V_c}{2\pi}\frac{A_0\,(c_{k0}+c_{r0})}{J_m}sz_e + \frac{T_m}{J_m},$$
$$(20)$$

$$\mathcal{L}\{F_a(t)\} = F_a(s) = A_0\Delta p + \frac{V_c}{2\pi}A_0\,(c_{k0}+c_{r0})\,\omega_m + A_0^2\,(c_{k0}+c_{r0})\,sz_e \quad (21)$$

where $\mathcal{L}\{\dot{z}_e(t)\} = sz_e(s)$ and $\mathcal{L}\{T_m(t)\} = T_m(s)$ are the Laplace transforms of the inputs. If we substitute Δp from equation (19) in (21) we obtain

$$F_a(s) = \left[A_0^2\,(c_{k0}+c_{r0})\,s + \kappa A_0^2\left(\frac{p_0}{V_{k0}} + \frac{p_0}{V_{r0}}\right)\right]z_e$$
$$+ \left[A_0^2\,(c_{k0}+c_{r0})\,s + \kappa A_0^2\left(\frac{p_0}{V_{k0}} + \frac{p_0}{V_{r0}}\right)\right]\frac{V_c}{2\pi A_0}\frac{\omega_m}{s}. \qquad (22)$$

Substitution of Δp from equation (20) in (21) results in

$$F_a(s) = -\frac{2\pi A_0 J_m}{V_c}s\omega_m + \frac{2\pi A_0}{V_c}T_m. \qquad (23)$$

Both equations can be simplified by introducing

$$z_m(s) = -\frac{V_c}{2\pi A_0}\frac{\omega_m}{s}\ , \quad \text{i.e.}\ \ z_m(t) = -\frac{V_c}{2\pi A_0}\int\omega_m, \quad F_m = \frac{2\pi A_0}{V_c}T_m \quad (24)$$

and the abbreviations

$$m = \left(\frac{2\pi}{V_c}\right)^2 A_0^2 J_m, \quad k = \kappa A_0^2\left(\frac{p_0}{V_{k0}} + \frac{p_0}{V_{r0}}\right), \quad c = A_0^2\,(c_{k0}+c_{r0}). \qquad (25)$$

Then, equations (22) and (23) read as

$$F_a(s) = (cs + k)\,(z_e - z_m), \qquad (26a)$$
$$F_a(s) = ms^2 z_m + F_m. \qquad (26b)$$

According to these two equations, the linear actuator model can be substituted by an equivalent mechanical system shown in Fig. 1b where (26b) represents the overall dynamics whereas (26a) corresponds to the spring-damper element. Obviously, the linearised actuator behaves like a single-mass system with natural frequency $\omega_0 = \sqrt{k/m}$ and damping ratio $\zeta = c/(2m\omega_0)$, where z_m is the internal position of the artificial actuator mass m, $z_e = z_r - z_a$ is the suspension deflection, and F_m represents the input force to the actuator.

    In the following, the controller design approach will be applied to a quarter-car model as shown in Fig. 1c, where z_a is the position of the sprung mass m_a, z_r is the position of the un-sprung mass m_r, k_a is the stiffness of the

suspension spring, k_r is the vertical tire stiffness, y_s is the road disturbance, and F_a represents the actuator force resulting from the actuator model in Fig. 1b. The dynamic behaviour for the quarter-car model can be obtained by applying the Newton's Second Law for the sprung and un-sprung mass. The resulting equations of motion read as

$$m_a \ddot{z}_a = F_a - k_a (z_a - z_r), \tag{27a}$$

$$m_r \ddot{z}_r = -F_a + k_a (z_a - z_r) - k_r (z_r - y_s). \tag{27b}$$

3. Control strategies

High damping forces are required to control the resonance peak of the sprung mass representing the car body, but high frequency performance may be degraded in this case. In order to solve this contradiction, often the ideal skyhook control is suggested as body controller. In such a suspension configuration the damper is virtually placed between sprung mass and inertial reference frame, i.e. the sky. In a practical implementation of such an approach, the active suspension has to apply forces which are proportional to the sprung mass velocity, resulting in the car body control law

$$F_{a,ref} = -\dot{z}_a C_{SH} \tag{28}$$

where C_{SH} is the skyhook damping parameter. The quantity $F_{a,ref}$ will be then the input reference force for the actuator controller. The objective of the skyhook control scheme is the cancellation of the sprung mass resonance peak, whereas for high frequencies it should be ineffective and perform similarly to a passive damper. The realisation of this goal, however, depends on the performance of the actuator controller and its ability to deal with high frequent disturbances. In the following, two classes of actuator controllers are designed and analysed in connection with the augmented quarter-car model: firstly two PID controllers and then a 2-DOF controller consisting of feed-forward and feedback path.

3.1. PID force controllers

Fig. 2a shows the principal structure of PID feedback control. The reference force $F_{a,ref}$ is compared to the measured output signal F_a to create an error signal acting as input of the PID controller. The output of the PID controller, which is equal to the input force F_m of the actuator in Fig. 1b, is a combination of three signals which are proportional to the error signal, its derivative and its integral.
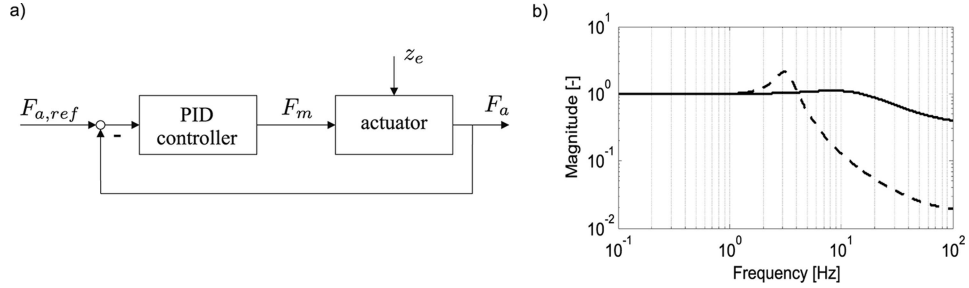
a)

b)

Fig. 2. Flowchart of the PID control approach (a) and (b) frequency responses of the high bandwidth (solid) and low bandwidth (dashed) controller

For the present application two different PID controllers were designed by loop-shaping, i.e. shaping the frequency response of the closed-loop system [10]. The first controller (PID-H) guarantees good tracking performance resulting from high closed-loop bandwidth. The second controller (PID-L) is designed as a compromise between achieving good tracking and having a bandwidth lower than the un-sprung mass mode. The frequency responses of both closed-loop systems are shown in Fig. 2b, where the transfer function is defined as

$$G_{cl} = \frac{F_a}{F_{a,ref}}.$$ (29)

We notice that the system with lower bandwidth exhibits a small resonance peak, suggesting a worse tracking performance than the system with the higher bandwidth even for low frequencies. The peak is inherently caused by the actuator's internal dynamics.

3.2. Two-degree-of-freedom controller

The second control approach is based on the internal model of the plant (26a) resulting in

$$z_m = z_e - \frac{F_a}{cs + k}.$$ (30)

Since the speed of the electric pump motor can be better controlled than its position, the velocity $v_m = sz_m$ is introduced resulting in the ideal feedforward control law

$$v_m = -\frac{s}{cs + k}F_a + sz_e.$$ (31)

For the real application, the exact actuator force F_a is substituted by the reference force $F_{a,ref}$ demanded by the body controller. In order to control the disturbance rejection, a disturbance controller

$$K_{dd} = sG_{tp}$$ (32)

composed of a derivator according to (31) and a low pass filter with transfer function G_{tp} is applied to the measured deflection signal $z_e(t)$. This results in the feed-forward control law for the reference velocity of the actuator

$$v_{m,ref} = -\frac{s}{cs + k} F_{a,ref} + K_{dd} z_e. \tag{33}$$

This reference actuator velocity is enforced by an internal PID feedback control loop, and additionally the reference force is weakly tracked by a PI-controller with transfer function K_{ss}, see Fig. 3. The two-degree-of-freedom control architecture allows us to shape reference and disturbance responses separately. The fast dynamics required for the reference tracking (solid black path) is decoupled from the low-gain feedback control law K_{ss} (dotted path) used to minimize the steady state error in the force. Further the disturbance rejection is regulated separately using the low-pass filter G_{tp} as part of K_{dd} (gray path). Here the right choice of the disturbance filter properties, including the order and the cut-off frequency, is very important for the active suspension performance. The velocity control loop may now be designed with high bandwidth, since by feedback of v_m contrarily to the force feedback control in Fig. 2a the high frequent content of the suspension force F_a will not disturb the controller. On the other hand the velocity control loop can be robust enough to eliminate actuator inertia effects of m and deal with eventual presence of friction in the motor-pump.
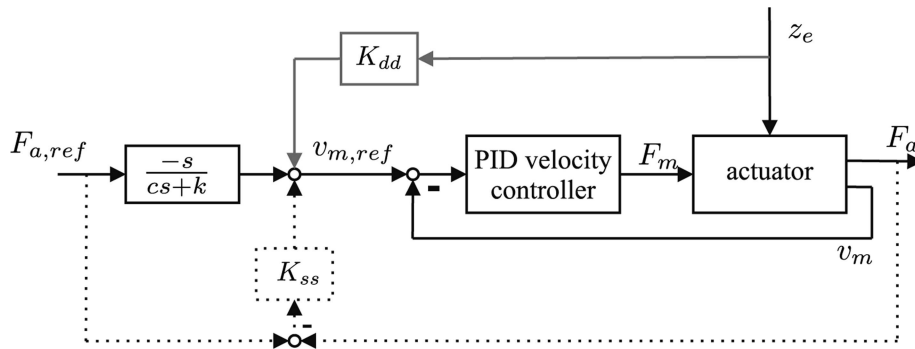

Fig. 3. Flowchart of the proposed linear 2-DOF control approach

The use of low-pass filter G_{tp} in (32) is motivated by the requirement to let the actuator behave like the passive system for high frequency deflections. Thus, the disturbance filter has to be designed such that measured low frequency disturbances are rejected while high frequent contents are ignored. In order to find a proper filter G_{tp} the closed-loop actuator dynamics in Fig. 3 is written as

$$F_a(s) = T(s) F_{a,ref}(s) + S(s) z_e(s) \tag{34}$$

where $T(s)$ determines the tracking behaviour and $S(s)$ represents the input-disturbance sensitivity. The bandwidth of the velocity control is high enough to assume $v_m \approx v_{m,ref}$ for low frequencies. Based on equation (26a) and $z_m = v_m/s$ we then assume that the output force of the controlled system is

$$F_a(s) = (cs + k)\left(z_e - \frac{v_{m,ref}}{s}\right). \tag{35}$$

From the control architecture in Fig. 3 the reference velocity input reads as

$$v_{m,ref} = \left(-\frac{s}{cs + k} + K_{ss}\right)F_{a,ref} - K_{ss}F_a + K_{dd}z_e. \tag{36}$$

Substituting (34) in (33), and the result in (32) yields the input-disturbance sensitivity

$$S(s) = \frac{K_{dd} - s}{K_{ss} - s/(cs + k)} \tag{37}$$

which describes the controlled actuator response on the deflection z_e. Let us now reconsider the passive system dynamics from equation (26a) for $z_m = 0$, i.e. $F_m \equiv F_a$, which then reads as

$$F_a(s) = (cs + k)z_e =: G_{d,p}(s)z_e \tag{38}$$

where $G_{d,p}(s) = (cs + k)$ is the passive disturbance response. The requirement to let the actuator (34) behave like the passive system (38) for high frequency deflections can be achieved by introducing a high-pass filter G_{hp}:

$$S \overset{!}{=} G_{hp}G_{d,p}. \tag{39}$$

This condition guarantees that high frequency disturbances have identical influence on the controlled actuator as on the passive system. Substituting (37), (38), and (32) in (39) yields

$$\frac{sG_{tp} - s}{K_{ss} - s/(cs + k)} = G_{hp}(cs + k). \tag{40}$$

Since K_{ss} is designed to be a low-gain controller, we may assume $|K_{ss}| \approx 0$ for high frequencies. This simplifies equation (40) to

$$G_{tp} = 1 - G_{hp}. \tag{41}$$

The high-pass filter G_{hp} with unity passband gain for high frequencies may be described by the transfer function

$$G_{hp} = \left(\frac{s}{2\pi f_c + s}\right)^n \tag{42}$$

where the cut-off frequency f_c in Hz and the order n have to be chosen properly.

3.3. Evaluation of the control systems

The linear quarter-car model (27) is considered for the evaluation of the proposed control systems. The road signal y_s represents the disturbance input, whereas the outputs involve the sprung mass acceleration $\ddot{z}_a$ and the dynamic tire load $k_r (z_r - y_s)$. The acceleration of the sprung mass is a suitable quantity for evaluating the motion and vibration of the car body, and thus can be used for assessing the driving comfort. Therefore, the transfer function between road disturbance and the sprung mass bounce acceleration is used to evaluate the effectiveness of the suspension system:

$$G_a(s) = \frac{s^2 z_a}{y_s}. \tag{43}$$

Furthermore, we use the dynamic tire load as an indicator for the road contact to evaluate the ride safety. It can be expressed in the frequency domain as:

$$G_{tl}(s) = k_r \frac{z_r - y_s}{y_s}. \tag{44}$$

Fig. 4 shows a comparison between the passive suspension (gray), i.e. $z_m = 0$, and three different active suspension configurations. Two of the active suspensions are controlled by the PID controllers from section 3.1, i.e. the high gain variant PID-H (dotted) and the low gain variant PID-L (dashed). For the third active suspension, the force control is generated by the 2-DOF controller (solid black) from the previous section.
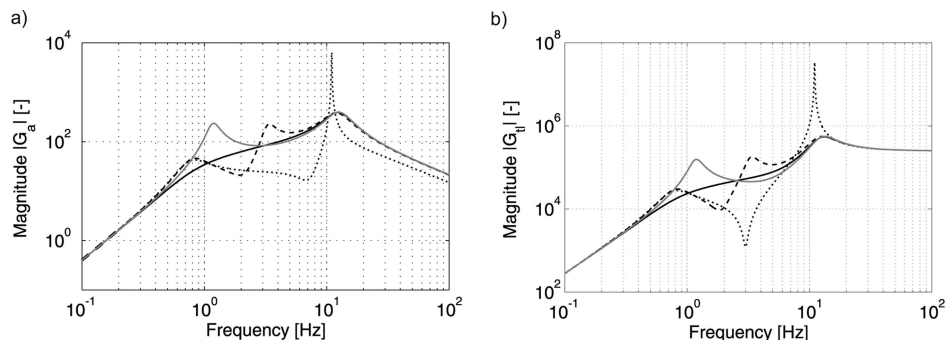

Fig. 4. Comparison of the sprung mass acceleration (a) and dynamic tire load (b) magnitudes for passive (gray), 2-DOF control (solid black), PID-H control (dotted), and PID-L control (dashed)

The linear frequency responses show that all three controllers produce similar results in reducing the bounce acceleration around the sprung mass

mode ($0.5 - 2$Hz), see Fig. 4a. However, the un-sprung mass mode for the PID-H controller shows an unacceptable resonance peak. This effect is the direct consequence of the high controller bandwidth, which ideally realizes the skyhook damping concept. Although the damping coefficient is larger than the built-in damper of the passive system, it is only applied to the small vibrations of the sprung mass, whereas the passive damper is related to the much bigger suspension deflections. As anticipated in the design phase, we notice that the PID-L controller with a bandwidth lower than the un-sprung mass mode has better high frequency properties. However, the resonance peak observed in Fig. 2b causes obvious deteriorations for middle frequencies at about 3Hz. Similar observations apply for the dynamic tire load plot in Fig. 4b, where we notice the presence of resonance peaks at 14Hz and 3Hz for the PID-H and PID-L conrollers, respectively. The proposed 2-DOF methodology results in globally better performance with a more uniform frequency response for the sprung mass acceleration as well as the dynamic tire load. It obviously guarantees the control objectives of damping low frequencies and having a response similar to that of the passive system for higher frequencies.

4. Nonlinear controller

The linearised model is valid only near the operating point and therefore not able to describe the behaviour of the nonlinear actuator in the whole operating range. By using the linear parameter-varying (LPV) system theory [11], however, the presented 2-DOF control approach can also be applied to the nonlinear actuator model. In contrast to linearization methods, the LPV model allows us to consider nonlinear effects in the state space description.

A continuous time linear parameter varying system can be written as

$$\dot{\boldsymbol{x}} = \boldsymbol{A}\left(\boldsymbol{\rho}\left(t\right)\right)\boldsymbol{x} + \boldsymbol{B}\left(\boldsymbol{\rho}\left(t\right)\right)\boldsymbol{u},$$
$$\boldsymbol{y} = \boldsymbol{C}\left(\boldsymbol{\rho}\left(t\right)\right)\boldsymbol{x} + \boldsymbol{D}\left(\boldsymbol{\rho}\left(t\right)\right)\boldsymbol{u} \tag{45}$$

where $\boldsymbol{\rho}\left(t\right)$ is a bounded time-varying parameter vector which can be measured online. In our case, the nonlinear state equations (16) can be re-interpreted as such a LPV system with time-varying parameters

$$\boldsymbol{\rho}\left(t\right) = \begin{bmatrix} \dfrac{p_{ks}}{V_{ks}} & \dfrac{p_{rs}}{V_{rs}} & c_k & c_r \end{bmatrix}^{T} = \begin{bmatrix} \dfrac{p_{ks}^{1+1/\kappa}}{V_{k0}p_0^{1/\kappa}} & \dfrac{p_{rs}^{1+1/\kappa}}{V_{r0}p_0^{1/\kappa}} & \bar{c}_k\left(q_m, \dot{z}_e\right) & \bar{c}_r\left(q_m, \dot{z}_e\right) \end{bmatrix} \tag{46}$$

where we assume that the states $p_{ks}(t)$, $p_{rs}(t)$, the input $\dot{z}_e(t)$ and the pump flow $q_m(t)$ are measurable. The second notation in equation (44) is obtained from equations (1), and (9) by substituting $V_{ks} = V_{k0}\left(p_0/p_{ks}\right)^{1/\kappa}$,

$V_{rs} = V_{r0}(p_0/p_{rs})^{1/\kappa}$ and $c_k(q_{ks}) = c_k(q_m + \dot{z}_e A_k) =: \bar{c}_k(q_m, \dot{z}_e)$, $c_r(q_{rs}) = c_r(-q_m - \dot{z}_e A_r) =: \bar{c}_r(q_m, \dot{z}_e)$. It is now possible to adapt the control part of Fig. 3 to the LPV system (43), where $\omega_{m,ref}$ in Fig. 5 corresponds to $v_{m,ref}$ in Fig. 3. Similarly to the linear concept, the inverted plant model leads to a control scheme combining feed-forward control (solid black path) with a disturbance rejection part (gray path). Further, a low-gain feedback control (dotted path) is added. We also notice that the control law takes into account the unsymmetrical system structure by distinguishing between the piston areas A_k and A_r.
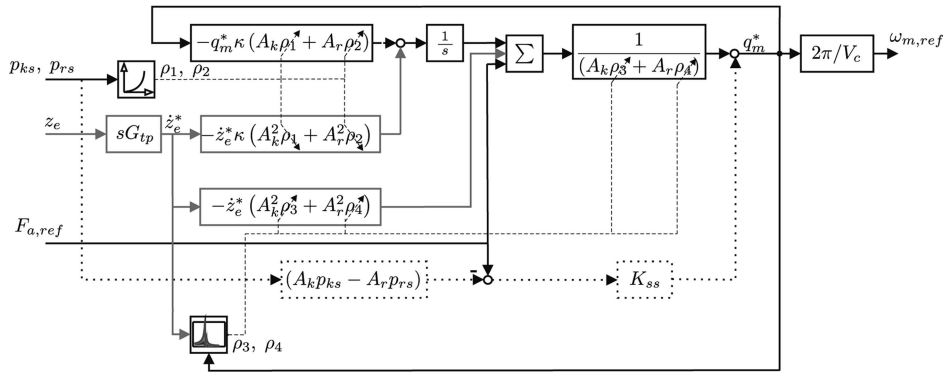

Fig. 5. Flowchart of the proposed nonlinear 2-DOF control approach

The presented control scheme for the nonlinear actuator was tested experimentally on a test rig. For this purpose, the actuator from Fig. 1a was excited by a second servo-hydraulic actuator, where a typical suspension deflection signal was used as displacement command signal. Moreover, a reference force signal served as input to the controller. Two experiments were realised. In the first experiment the passive system, i.e. $\omega_m = 0$, was excited, whereas the second experiment involved the controlled actuator. The measurements in Fig. 6b show that a good reference tracking performance is achieved for low frequent force components when the control system is activated. The high frequent differences, which are responsible for the damping of the unsprung mass mode, are almost identical to those of a passive damper as shown in Fig. 6a and predicted by the frequency response in Fig. 4. The experimental results confirm that the control objectives set in the design phase are accomplished for the real nonlinear system as well.

5. Full-car control

The 2-DOF control approach from the previous section was implemented in a test car. Therefore, it was required to adapt the car body control law
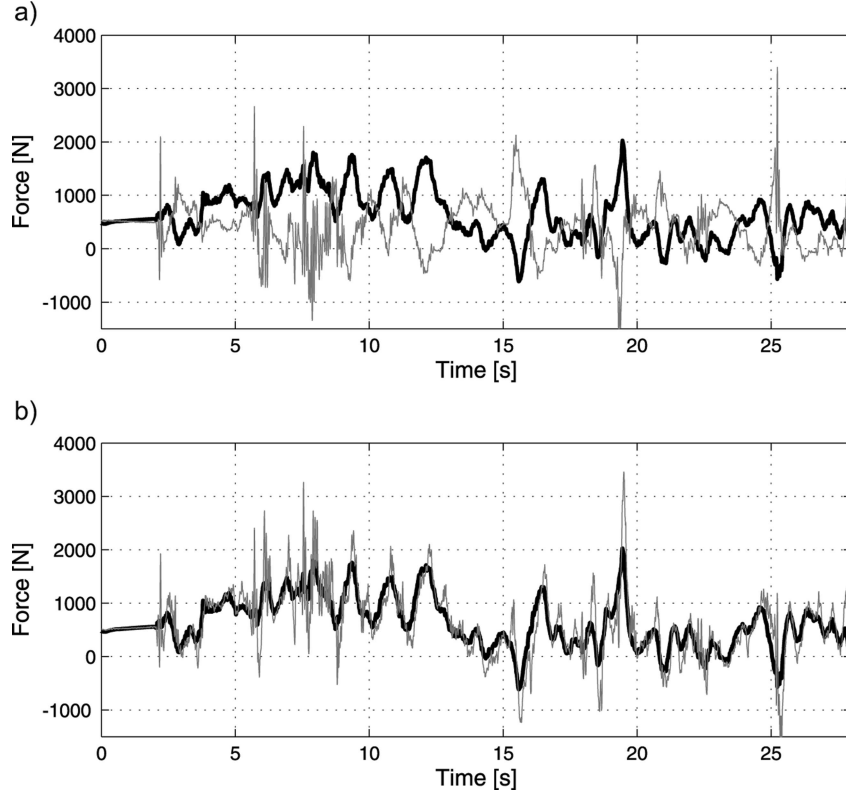
a)

b)

Fig. 6. Comparison between reference force test signal (black) and measured force signal (gray)
for the passive (a) and controlled (b) actuator

(27) to the full-car framework. Fig. 7 shows a linear vertical full-car model
used for the full-car body controller design. The model consists of a spatial
sprung mass connected to four un-sprung masses at each corner. A modal
control strategy is used to control the car body. In such a configuration,
the modal motions heave z_H, roll φ_R and pitch φ_P are to be assessed and
controlled. Especially, the first derivatives of the modal states are used to
calculate virtual skyhook forces and moments as

$$\boldsymbol{F}_V = \begin{bmatrix} F_H \\ M_R \\ M_P \end{bmatrix} = \begin{bmatrix} -\dot{z}_H C_{SH,H} \\ -\dot{\varphi}_R C_{SH,R} \\ -\dot{\varphi}_P C_{SH,P} \end{bmatrix} \qquad (47)$$

where $C_{SH,H}$, $C_{SH,R}$, and $C_{SH,P}$ are the skyhook damping parameters for
heave, roll and pitch, respectively. The virtual modal quantities are then
distributed to reference forces for the four active actuators

$$\boldsymbol{F}_{a,ref} = \begin{bmatrix} F_{a,ref,fl} & F_{a,ref,fr} & F_{a,ref,rl} & F_{a,ref,rr} \end{bmatrix} = \boldsymbol{M}\boldsymbol{F}_V \qquad (48)$$

where

$$\boldsymbol{M} = \frac{1}{(l_f + l_r)(w_f + w_r)} \begin{bmatrix} l_r w_r & l_r & -w_r \\ l_r w_l & -l_r & -w_l \\ l_f w_r & l_f & w_r \\ l_f w_l & -l_f & -w_l \end{bmatrix} \quad (49)$$

is a static distribution matrix. The reference force signals (48) serve as an input to the actuator controllers which are duplications of the nonlinear controller from Fig. 5. The pressures in the accumulators, as well as the suspension deflection for each corner, are measured and fed back to the controllers to calculate the reference angular velocity signals for the electric motors.
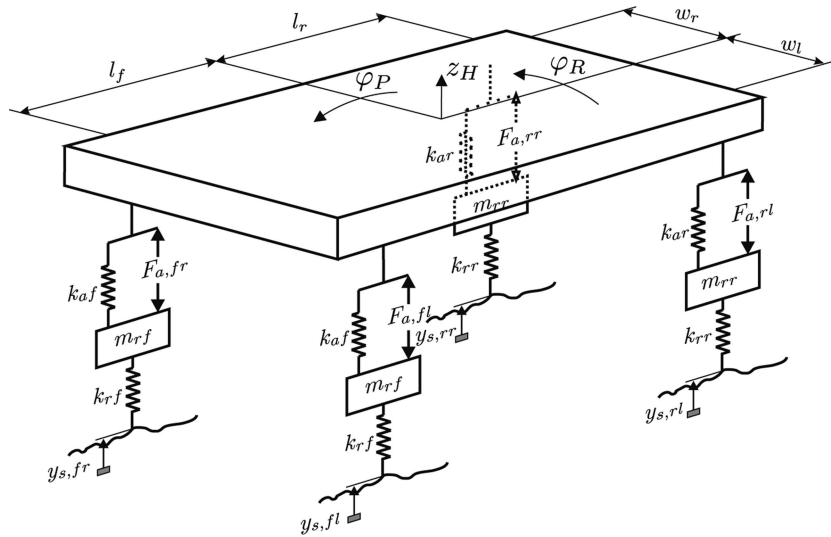

Fig. 7. Linear full-car model

A test car was equipped with this soft- and hardware, and then driven over the test track at a speed of 70 km/h. In subsequent trials, different configurations were tested. The first configuration consists of the passive suspension with a soft valves setting, whereas in the second configuration the damping valves are set to the hard mode. Of more interest is actually the third configuration, in which the active mode with the nonlinear actuator controller is used.

For the evaluation of the nonlinear model, a normalized power spectral density (PSD) analysis is applied to the modal acceleration signals $\ddot{z}_H$, $\ddot{\varphi}_R$ and $\ddot{\varphi}_P$. The results in Fig. 8 show that the passive system with the hard setting (dashed) achieves a considerable reduction of the bounce accelerations around the sprung mass mode. However, for higher frequencies we simultaneously notice performance deterioration, especially for the sensitive

middle frequencies (2 − 8Hz). As already anticipated, the active system (solid black) performs best and achieves the design requirements of reducing low frequency accelerations while performing similarly to the soft passive system (gray) at high frequencies. We notice similarities with the frequency response of the linear systems in Fig. 4, and that frequency regions with significant vibration reduction are also confirmed by the nonlinear PSD analysis.
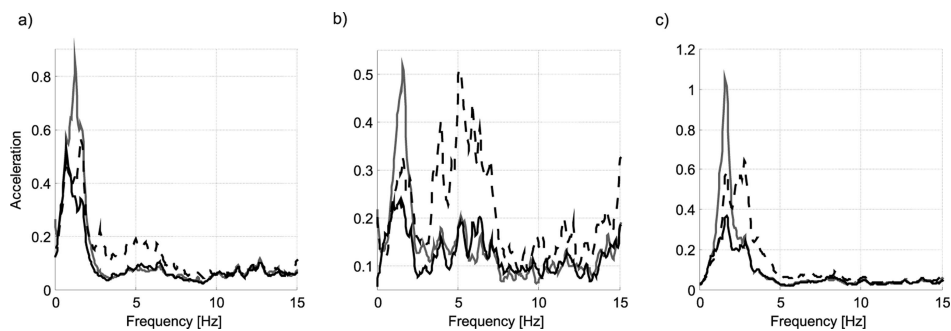

Fig. 8. PSD analysis of the test car body modal accelerations heave (a), roll (b), and pitch (c) for the following suspension configurations: passive with soft damping (gray), passive with hard damping (dashed), and active with the nonlinear 2-DOF controller (solid black)

6. Conclusions and outlook

The control approach presented in this paper is derived based on a linearised and reduced model of the control plant. This allows us to evaluate two different controller concepts in the frequency domain, where the 2-DOF controller achieves a superior performance compared to two different types of PID controllers. Considering this result and a LPV representation of the nonlinear model, a nonlinear 2-DOF controller is developed and tested on an experimental test rig. The measurements show a promising force tracking performance associated with a good disturbance response. These results have then been confirmed by measurements on a real test car, which shows a considerable ride performance improvement using the active suspension system. The two-degree-of-freedom control achieves a remarkable reduction of low frequency vibrations while keeping the same level as the soft passive damper for higher frequencies. The current work of the authors involves extending the presented control concept with a preview approach to achieve more efficiency [12], and to also implement it in the test car.

REFERENCES

[1] Cao J., Liu H., Li P., Brown D.J.: State of the Art in Vehicle Active Suspension Adaptive Control Systems Based on Intelligent Methodologies. IEEE Transactions on Intelligent Transportation Systems, Vol. 9, pp. 392-405, 2008.

[2] Cao D., Song S., Ahmadian M.: Editors's Perspectives: Road Vehicle Suspension Design, Dynamics, and Control. Vehicle System Dynamics, Vol. 49, pp. 3-28, 2011.

[3] Esmailzadeh E., Taghirad H.D.: State-Feedback Control for Passenger Ride Dynamics. The Transactions of the Canadian Society for Mechanical Engineering, Vol. 19, pp. 495-508, 1995.

[4] Fialho I., Balas G.J.: Road Adaptive Active Suspension Design Using Linear Parameter-Varying Gain-Scheduling. IEEE Transactions on Control Systems Technology, Vol. 10, pp. 43-54, 2002.

[5] Du H., Zhang N.: Constrained H_∞ Control of Active Suspension for a Half-car Model with a Time Delay in Control. Proceedings of IMechE, Part D: Journal of Automobile Engineering, Vol. 222, pp. 665-508, 2008.

[6] Bluethmann B., Herrera E., Hulse A., Figuered J., Junkin L., Markee M., Ambrose R.O.: An Active Suspension System For Lunar Crew Mobility. IEEE Aerospace Conference, Big Sky, MT, USA, pp. 1-9, 2010.

[7] Lauwerys C., Swevers J., Sas P.: Linear Control of Car Suspension Using Nonlinear Actuator Control. Proceedings of the International Conference on Noise and Vibration Engineering, Leuven, Belgium, pp. 55-61, 2002.

[8] Koch G., Fritsch O., Lohmann B.: Potential of Low Bandwidth Active Suspension Control with Continuously Variable Damper. Proceedings of the 17th IFAC World Congress, Seoul, Korea, pp. 3392-3397, 2008.

[9] Cytrynski S.: Federungssystem für ein Fahrzeug. Patent DE102010007237A1, 2010.

[10] Cominos P., Munro N.: PID Controllers: Recent Tuning Methods and Design to Specification. IEE Proceedings – Control Theory and Applications, Vol. 149, pp. 46-53, 2002.

[11] Kamen E.W., Khargonekar P.P.: On the Control of Linear Systems whose Coefficients Are Functions of Parameters. IEEE Transactions on Automatic Control, Vol. 29, pp. 25-23, 1984.

[12] Ajala O., Bestle D., Rauh J., Ammon D.: Zero-phase Filtering Control of an Active Suspension System with Preview. Proceedings of the 11th International Symposium on Advanced Vehicle Control, Seoul, Korea, 2012.

Modelowanie i sterowanie aktywnego, hydro-elektrycznego systemu zawieszenia

S t r e s z c z e n i e

Aktywne systemy zawieszenia łagodzą konflikt między komfortem a właściwościami jezdnymi samochodu. Wymagają one użycia odpowiednich siłowników, a te z kolei powinny być efektywnie sterowane. W artykule zaproponowano opartą na modelowaniu koncepcję sterowania nieliniowego siłownika w zawieszeniu samochodu. Koncepcja tego rozwiązania jest początkowo przedstawiona w ramach opisu liniowego, co ma uprościć fazę syntezy i analizy. Na tym etapie jest proponowany i dyskutowany model liniowy. Ta faza projektowania obejmuje ponadto porównanie między niezwiązanymi z modelem sterownikami PID i proponowanym, nowym sterownikiem o dwu stopniach swobody, który pozwala niezależnie kształtować odpowiedź referencyjną i odpowiedź na zakłócenia. W dalszym etapie, dla sterownika o dwu stopniach swobody, który okazał się lepszy od pozostałych, wprowadza się opis nieliniowy, traktując parametr liniowy jak zmienną reprezentację nieliniowego obiektu regulacji. Ostatecznie, nieliniowy sterownik zawieszenia jest instalowany w samochodzie testowym, a badania potwierdzają celowość zastosowania tej koncepcji w rzeczywistym sprzęcie.